Fast numerical method for electromagnetic scattering by rough layered interfaces: Propagation-inside-layer expansion method

Nicolas Déchamps, Nicole de Beaucoudrey, Christophe Bourlier, and Serge Toutain

IREENA, Ecole Polytechnique de l'Université de Nantes, Rue Christian Pauc, La Chantrerie, BP 50609, 44306 Nantes cedex 3, France

Received June 8, 2005; accepted July 22, 2005

Electromagnetic scattering from a stack of two one-dimensional rough surfaces separating homogeneous media is modeled with a rigorous integral formulation solved by the method of moments. We present an efficient numerical method for computing the field scattered by such rough layers, in reflection as well as in transmission. We call this method propagation-inside-layer expansion (PILE) due to its straightforward physical interpretation. To our knowledge, it is the first method able to handle problems for this configuration with a huge number of unknowns. We study the convergence of this method versus a coupling condition and validate it by comparison with results from the literature. © 2006 Optical Society of America

OCIS codes: 290.5880, 290.4210, 280.0280.

1. INTRODUCTION

The study of electromagnetic scattering by layered rough surfaces has a large number of applications in, for example, optics for coated surfaces,[1–9] remote sensing for the monitoring of oil spills,[10] and detection of buried interfaces (e.g., in sediments) using ground-penetrating radar.[11]

Of particular interest are integral methods to derive the field scattered by surfaces separating homogeneous media. These methods can rigorously lead to knowledge of the scattered field, which is not the case when using asymptotic methods[12–14] such as the Kirchhoff approximation or the small-perturbation method. Integral methods aim at obtaining the total field and/or its normal derivative on the surfaces: These surface unknowns are linked to the incident field by means of integral equations, and the method of moments (MoM)[15,16] transforms these integral equations in a linear system.

For the case of a *single* rough surface, "fast" methods of resolution of this linear system have been developed in order to reduce the number of operations as well as the memory storage space.[13,14,16] When one considers a stack of *two* rough surfaces, the number of unknowns is increased. Consequently, fast methods are of particular interest for this configuration but, to our knowledge, have not been developed until now for the two-dimensional problem. Hence, the use of integral methods for a stack of two surfaces is restricted to surfaces sampled on a coarse grid, in order to deal with a lower number of unknowns.[17,18] This basic numerical limitation made a great number of studies intractable until now.

To overcome this limitation, we propose a fast numerical method,[19] which is devoted to efficiently computing the scattering from a stack of two one-dimensional rough interfaces. Due to its straightforward physical interpretation, we choose to call this approach the propagation-inside-layer expansion (PILE) method. This paper is organized as follows: In Section 2, we recall the integral equations derived for a stack of two rough interfaces and the linear system obtained by the MoM. Section 3 describes the PILE method, which efficiently inverts the linear system; its validity domain is studied next, as well as a preconditioning technique. In Section 4, we validate this new method by comparison with results given in the literature.

2. INTEGRAL FORMULATION FOR A ROUGH LAYER

A. Rough Layer and Incident Beam

Let us assume that the rough layer is invariant along the $\hat{\mathbf{y}}$ direction and that the incident wave vector is lying in the $(\hat{\mathbf{x}},\hat{\mathbf{z}})$ plane. Consequently, the problem is two dimensional, and the layer is delimited by two one-dimensional surfaces: an upper one, S^+, defined by the surface equation $z=\zeta^+(x)$, and a lower one, S^-, defined by $\zeta^-(x)$ (Fig. 1). $\zeta^\pm(x)$ are assumed to be stochastic, stationary, Gaussian processes, satisfying $\langle\zeta^+\rangle=0$ and $\langle\zeta^-\rangle=-H$, where $H>0$ is the mean layer thickness; the surface height spectrum can be of any kind: Gaussian, West–O'Donnell,[20] etc. If the surfaces are not identical, one must pay special attention to avoid any intersection of them.

The surfaces separate three homogeneous media: the upper one, Ω_0, considered air; the intermediate one, Ω_1, filling the layer; and the lower one, Ω_2. Ω_2 will be considered a lossy dielectric or a perfect conductor, and we will refer to the corresponding configuration, for the sake of simplicity, as a dielectric case or a perfectly conducting case.

The random surfaces $S^\pm$ can easily be generated by a spectral method, widely used in the calculation of wave scattering.[16] If N represents the number of samples for each surface, discretized abscissa and heights of the surfaces are given by

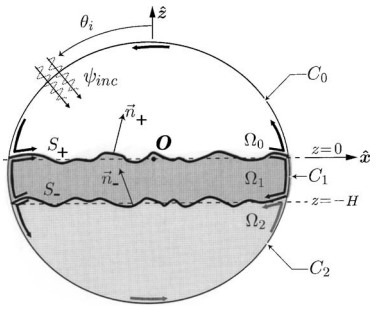

Fig. 1. Geometry of the problem and contour integration paths.

$$x_n = -\frac{L}{2} + \left(n - \frac{1}{2}\right)\Delta x, \qquad \zeta^{\pm}(x_n), \qquad n = 1, \ldots, N, \quad (1)$$

where $\Delta x = L/N$ is the sampling step and L is the total length of each surface. A point of the plane $(\hat{\mathbf{x}}, \hat{\mathbf{z}})$ will be denoted by $\mathbf{r} = x\hat{\mathbf{x}} + z\hat{\mathbf{z}}$, and a point of $S^{\pm}$ by $\mathbf{r}_n^{\pm} = x_n\hat{\mathbf{x}} + \zeta^{\pm}(x_n)\hat{\mathbf{z}}$.

To avoid edge limitations, we choose the incident field ψ_{inc} as a Thorsos tapered plane wave.[21] Let us denote the incident angle as θ_i, defined with respect to $\hat{\mathbf{z}}$ in the counterclockwise direction, and the tapering parameter as g, which has a dimension of length and controls the spatial extent of the incident wave. Typically, g is chosen to be some fraction of L; we used $g = L/6$ or $g = L/10$ in numerical simulations. Furthermore, we consider both TE (or s) and TM (or p) polarizations. An $e^{j\omega t}$ time-harmonic convention is used.

As we consider homogeneous media, we choose the frame of surface integral methods. Integral equations have been established for perfectly conducting[17] and lossy dielectric[18,22] lower media. We successively present the dielectric (Subsection 2.B) and perfectly conducting (Subsection 2.C) cases.

B. Dielectric Case

1. Integral Equations

Let us define $\{\psi_j\}_{j=0,1,2}$ as the total field in each medium Ω_j. The purpose of integral methods is to evaluate the fields and their first derivatives onto $S^{\pm}$ and then, by means of Huygens's principle, to deduce the scattered field in each medium.

For $\mathbf{r}$ located on the rough surfaces, the fields $\{\psi_j\}_{j=0,1,2}$ satisfy the following boundary conditions:

$$\psi_0(\mathbf{r})\big|_{\mathbf{r}\in S_+} = \psi_1(\mathbf{r})\big|_{\mathbf{r}\in S_+},$$

$$\left.\frac{\partial\psi_0(\mathbf{r})}{\partial n_+}\right|_{\mathbf{r}\in S_+} = \frac{1}{\rho_{10}}\left.\frac{\partial\psi_1(\mathbf{r})}{\partial n_+}\right|_{\mathbf{r}\in S_+}, \quad (2a)$$

$$\psi_1(\mathbf{r})\big|_{\mathbf{r}\in S_-} = \psi_2(\mathbf{r})\big|_{\mathbf{r}\in S_-},$$

$$\left.\frac{\partial\psi_1(\mathbf{r})}{\partial n_-}\right|_{\mathbf{r}\in S_-} = \frac{1}{\rho_{21}}\left.\frac{\partial\psi_2(\mathbf{r})}{\partial n_-}\right|_{\mathbf{r}\in S_-}, \quad (2b)$$

where $\rho_{10} = \rho_{21} = 1$ in the TE case and $\rho_{10} = \varepsilon_1/\varepsilon_0$, $\rho_{21} = \varepsilon_2/\varepsilon_1$ in the TM case. The upward normal $\mathbf{n}_{\pm}$ to the surface $S_{\pm}$ is defined as

$$\mathbf{n}_{\pm} = \frac{-\zeta'_{\pm}\hat{\mathbf{x}} + \hat{\mathbf{z}}}{\sqrt{1 + (\zeta'_{\pm})^2}},$$

where $\zeta'_{\pm} = \partial\zeta_{\pm}/\partial x$.

Let us consider three contour paths of integration, C_0, C_1, and C_2, represented in Fig. 1. Applying Green's theorem under the assumption that the fields ψ_j and their normal derivatives $\partial\psi_j/\partial n_{\pm}$ on both interfaces are negligible at the edges, we obtain four coupled equations. When the boundary conditions (2) are introduced, these four equations, linking the incident field ψ_{inc} and the total fields ψ_0 and ψ_1 on the rough surfaces S_+ and S_-, become

$$\underbrace{\frac{1}{2}\psi_0(\mathbf{r}') - \int_{S_+} ds\, \psi_0(\mathbf{r})\frac{\partial g_0(\mathbf{r}',\mathbf{r})}{\partial n_+}}_{\mathbf{A}^+} + \underbrace{\int_{S_+} ds\, g_0(\mathbf{r}',\mathbf{r})\frac{\partial\psi_0(\mathbf{r})}{\partial n_+}}_{\mathbf{B}^+} = \psi_{inc}(\mathbf{r}'), \qquad \mathbf{r}' \in S_+, \quad (3a)$$

$$\underbrace{-\frac{1}{2}\psi_0(\mathbf{r}') - \int_{S_+} ds\, \psi_0(\mathbf{r})\frac{\partial g_1(\mathbf{r}',\mathbf{r})}{\partial n_+}}_{\mathbf{C}^+} + \underbrace{\int_{S_+} ds\, g_1(\mathbf{r}',\mathbf{r})\frac{\partial\psi_0(\mathbf{r})}{\partial n_+}\rho_{10}}_{\rho_{10}\mathbf{D}^+} + \underbrace{\int_{S_-} ds\left[\psi_1(\mathbf{r})\frac{\partial g_1(\mathbf{r}',\mathbf{r})}{\partial n_-}\right.}_{\mathbf{E}} \underbrace{\left. - g_1(\mathbf{r}',\mathbf{r})\frac{\partial\psi_1(\mathbf{r})}{\partial n_-}\right]}_{\mathbf{F}} = 0, \qquad \mathbf{r}' \in S_+, \quad (3b)$$

$$\underbrace{\int_{S_+} ds\left[\psi_0(\mathbf{r})\frac{\partial g_1(\mathbf{r}',\mathbf{r})}{\partial n_+}\right.}_{\mathbf{G}} \underbrace{\left. - g_1(\mathbf{r}',\mathbf{r})\frac{\partial\psi_0(\mathbf{r})}{\partial n_+}\rho_{10}\right]}_{\rho_{10}\mathbf{H}} + \underbrace{\frac{1}{2}\psi_1(\mathbf{r}') - \int_{S_-} ds\, \psi_1(\mathbf{r})\frac{\partial g_1(\mathbf{r}',\mathbf{r})}{\partial n_-}}_{\mathbf{A}^-} + \underbrace{\int_{S_-} ds\, g_1(\mathbf{r}',\mathbf{r})\frac{\partial\psi_1(\mathbf{r})}{\partial n_-}}_{\mathbf{B}^-} = 0, \qquad \mathbf{r}' \in S_-, \quad (3c)$$

$$\underbrace{-\frac{1}{2}\psi_1(\mathbf{r}') - \int_{S_-} ds\, \psi_1(\mathbf{r})\frac{\partial g_2(\mathbf{r}',\mathbf{r})}{\partial n_-}}_{\mathbf{C}^-} + \underbrace{\int_{S_-} ds\, g_2(\mathbf{r}',\mathbf{r})\frac{\partial\psi_1(\mathbf{r})}{\partial n_-}\rho_{21}}_{\rho_{21}\mathbf{D}^-} = 0, \qquad \mathbf{r}' \in S_-. \quad (3d)$$

In these expressions, $\fint_S ds$ is the principal value integral. The Green functions of regions Ω_j are expressed by

$$g_j(\mathbf{r}',\mathbf{r}) = \frac{i}{4}H_0^{(1)}(k_j\|\mathbf{r} - \mathbf{r}'\|), \quad (4)$$

where k_0 is the wave number in free space and $\{k_{1,2}\}$ denote the wave numbers in the inner and lower media. $H_0^{(1)}(\cdot)$ is the zeroth-order Hankel function of the first kind. The meaning of symbols **A** to **H** will be given below.

2. Discretization by the Method of Moments

We apply the MoM with point matching and pulse basis functions.[15] From boundary conditions (2) and the set of integral equations (3), we obtain a linear system of the form $\mathbf{Z}\cdot\mathbf{X}=\mathbf{b}$, where the unknown vector $\mathbf{X}$ is equal to

$$\mathbf{X}_{4N\times 1}=\begin{bmatrix}\mathbf{X}_+\\ \mathbf{X}_-\end{bmatrix}, \tag{5}$$

with $\mathbf{X}_+$ and $\mathbf{X}_-$ containing the unknown fields and their normal derivatives on the upper and lower surfaces, respectively. They have the following expressions:

$$\mathbf{X}_+^{\mathrm{t}}=\begin{bmatrix}\psi_0(\mathbf{r}_1^+)\cdots\psi_0(\mathbf{r}_N^+) & \dfrac{\partial\psi_0(\mathbf{r}_1^+)}{\partial n_+}\cdots\dfrac{\partial\psi_0(\mathbf{r}_N^+)}{\partial n_+}\end{bmatrix}, \tag{6}$$

$$\mathbf{X}_-^{\mathrm{t}}=\begin{bmatrix}\psi_1(\mathbf{r}_1^-)\cdots\psi_1(\mathbf{r}_N^-) & \dfrac{\partial\psi_1(\mathbf{r}_1^-)}{\partial n_-}\cdots\dfrac{\partial\psi_1(\mathbf{r}_N^-)}{\partial n_-}\end{bmatrix}, \tag{7}$$

where $\mathbf{X}^{\mathrm{t}}$ stands for the transpose of $\mathbf{X}$.

The source term $\mathbf{b}$ contains the information about the incident field:

$$\mathbf{b}_{4N\times 1}=\begin{bmatrix}\mathbf{b}_+\\ \mathbf{b}_-\end{bmatrix}=\Big[\underbrace{\psi_{inc}(\mathbf{r}_1^+)\cdots\psi_{inc}(\mathbf{r}_N^+)\quad 0\cdots 0}_{\mathbf{b}_+^{\mathrm{t}}}\quad\underbrace{0\cdots 0\quad 0\cdots 0}_{\mathbf{b}_-^{\mathrm{t}}}\Big]^{\mathrm{t}}. \tag{8}$$

The impedance matrix has the form

$$\mathbf{Z}_{4N\times 4N}=\begin{bmatrix}\mathbf{Z}^U & \mathbf{C}^U\\ \mathbf{C}^L & \mathbf{Z}^L\end{bmatrix}, \tag{9}$$

where $\mathbf{Z}^U$, $\mathbf{Z}^L$, $\mathbf{C}^U$, and $\mathbf{C}^L$ are square matrices of size $2N\times 2N$:

$$\mathbf{Z}^U_{2N\times 2N}=\begin{bmatrix}\mathbf{A}^+ & \mathbf{B}^+\\ \mathbf{C}^+ & \rho_{10}\mathbf{D}^+\end{bmatrix},\qquad \mathbf{Z}^L_{2N\times 2N}=\begin{bmatrix}\mathbf{A}^- & \mathbf{B}^-\\ \mathbf{C}^- & \rho_{21}\mathbf{D}^-\end{bmatrix}, \tag{10}$$

$$\mathbf{C}^U_{2N\times 2N}=\begin{bmatrix}\mathbf{0} & \mathbf{0}\\ \mathbf{E} & \mathbf{F}\end{bmatrix},\qquad \mathbf{C}^L_{2N\times 2N}=\begin{bmatrix}\mathbf{G} & \rho_{10}\mathbf{H}\\ \mathbf{0} & \mathbf{0}\end{bmatrix}. \tag{11}$$

The superscript U stands for "upper," and L for "lower." $\mathbf{Z}^U$ exactly corresponds to the impedance matrix of a single-interface problem,[16] where the interface considered is the upper one (S^+). Likewise, $\mathbf{Z}^L$ is the impedance matrix of the single surface S^-. Moreover, matrices $\mathbf{C}^U$ and $\mathbf{C}^L$ can be seen as coupling matrices between the two interfaces S^+ and S^-. Actually, according to integral equation (3b), $\mathbf{C}^U$ propagates information from the lower interface toward the upper one ($S^-\rightarrow S^+$). The same remark holds for matrix $\mathbf{C}^L$: It is the coupling matrix from the upper surface toward the lower one ($S^+\rightarrow S^-$).

$\mathbf{A}^\pm$, $\mathbf{B}^\pm$, $\mathbf{C}^\pm$, $\mathbf{D}^\pm$, $\mathbf{E}$, $\mathbf{F}$, $\mathbf{G}$, and $\mathbf{H}$ are derived by discretizing Eqs. (3) and are given in Appendix A. Each of these 16 blocks of $\mathbf{Z}$ has a size of $N\times N$, the four blocks in Eq. (9) have a size of $2N\times 2N$, and so the size of $\mathbf{Z}$ is $4N\times 4N$, with $4(N\times N)$ zero elements contained in the $\mathbf{C}^U$ and $\mathbf{C}^L$ matrices.

C. Perfectly Conducting Case

When the lower medium is perfectly conducting, in expression (9) of the impedance matrix $\mathbf{Z}$, $\mathbf{Z}^U$ is obviously identical to that in the dielectric case. Differences arise in $\mathbf{Z}^L$, which is reduced to an $N\times N$ matrix, and from the coupling matrices, which are no longer square. For TE polarization, we get

$$\mathbf{Z}^L_{N\times N}=\mathbf{B}^-,\quad \mathbf{C}^U_{2N\times N}=\begin{bmatrix}\mathbf{0}\\ \mathbf{F}\end{bmatrix},\qquad \mathbf{C}^L_{N\times 2N}=[\mathbf{G}\quad \rho_{10}\mathbf{H}], \tag{12}$$

and for TM polarization, we obtain

$$\mathbf{Z}^L_{N\times N}=\mathbf{A}^-,\qquad \mathbf{C}^U_{2N\times N}=\begin{bmatrix}\mathbf{0}\\ \mathbf{E}\end{bmatrix},\qquad \mathbf{C}^L_{N\times 2N}=[\mathbf{G}\quad \rho_{10}\mathbf{H}]. \tag{13}$$

Impedance matrice $\mathbf{Z}$ is of size $3N\times 3N$, and the unknowns are $[\psi_0,\partial\psi_0/\partial n_+,\partial\psi_1/\partial n_-]$ in the TE case and $[\psi_0,\partial\psi_0/\partial n_+,\psi_1]$ in the TM case.

D. Scattered Field and Bistatic Cross Section

Once the equation $\mathbf{Z}\cdot\mathbf{X}=\mathbf{b}$ is solved for $\mathbf{X}$, we can derive, using Huygens's principle,[16] the scattered fields $\{\psi_j\}_{j=0,1,2}$ in the media Ω_j:

- ψ_0 in the upper medium Ω_0, from the values $\mathbf{X}_+=[\psi_0,\partial\psi_0/\partial n_+]$ on the upper surface S_+;
- ψ_2 in the lower medium Ω_2, from $\mathbf{X}_-$;
- ψ_1 in the inner medium Ω_1, from both $\mathbf{X}_+$ and $\mathbf{X}_-$, by using the following expression, valid for $\mathbf{r}'\in\Omega_1$:

$$\psi_{sc}(\mathbf{r}')=\int_{S^+}\mathrm{d}s^+\left[\psi_0(\mathbf{r}^+)\frac{\partial g_1(\mathbf{r}^+,\mathbf{r}')}{\partial n^+}-g_1(\mathbf{r}^+,\mathbf{r}')\frac{\partial\psi_0(\mathbf{r}^+)}{\partial n^+}\right]-\int_{S^-}\mathrm{d}s^-\left[\psi_1(\mathbf{r}^-)\frac{\partial g_1(\mathbf{r}^-,\mathbf{r}')}{\partial n^-}-g_1(\mathbf{r}^-,\mathbf{r}')\frac{\partial\psi_1(\mathbf{r}^-)}{\partial n^-}\right]. \tag{14}$$

Finally, the bistatic cross section (BCS), also known as the mean differential reflection coefficient, can be derived in the far field.[16,17,23]

3. PROPAGATION-INSIDE-LAYER EXPANSION: FAST METHOD FOR A ROUGH LAYER

Until now, no efficient method has been available to achieve a fast resolution of the equation $\mathbf{Z}\cdot\mathbf{X}=\mathbf{b}$, unlike for the single-interface problem. Hence, a direct inversion of $\mathbf{Z}$ has to be used, with limitation to a maximal number of samples on each surface, typically around $N\simeq 800$ for a personal computer (2 GHz processor, 1 Gbit RAM). This illustrates the particular interest in developing efficient and fast numerical methods, requiring low memory space, for the resolution of $\mathbf{Z}\cdot\mathbf{X}=\mathbf{b}$ in the case of a rough layer. Indeed, our method[19] takes advantage of the block partitioning of the impedance matrix (9).

A. Efficient Algorithm

The algorithm is presented here in the general dielectric case. Let us assume that we already have the inverse matrix $\mathbf{Z}^{-1}$; we can partition it into four blocks:

$$\mathbf{Z}^{-1} = \begin{bmatrix} \mathbf{T} & \mathbf{U} \\ \mathbf{V} & \mathbf{W} \end{bmatrix}, \tag{15}$$

where the square matrices $\mathbf{T}$, $\mathbf{U}$, $\mathbf{V}$, and $\mathbf{W}$ are of size $2N \times 2N$ and can be expressed[24] with the four blocks of $\mathbf{Z}$ given in Eq. (9) as follows:

$$\mathbf{T} = [\mathbf{Z}^U - \mathbf{C}^U \cdot (\mathbf{Z}^L)^{-1} \cdot \mathbf{C}^L]^{-1}, \tag{16a}$$

$$\mathbf{U} = -\mathbf{T} \cdot \mathbf{C}^U \cdot (\mathbf{Z}^L)^{-1}, \tag{16b}$$

$$\mathbf{V} = -(\mathbf{Z}^L)^{-1} \cdot \mathbf{C}^L \cdot \mathbf{T}, \tag{16c}$$

$$\mathbf{W} = (\mathbf{Z}^L)^{-1} - (\mathbf{Z}^L)^{-1} \cdot \mathbf{C}^L \cdot \mathbf{T} \cdot \mathbf{C}^U \cdot (\mathbf{Z}^L)^{-1}. \tag{16d}$$

From Eq. (15), the unknowns $\mathbf{X}$ are given by

$$\begin{pmatrix} \mathbf{X}_+ \\ \mathbf{X}_- \end{pmatrix} = \mathbf{Z}^{-1} \begin{pmatrix} \mathbf{b}_+ \\ \mathbf{b}_- \end{pmatrix} = \begin{pmatrix} \mathbf{T} \cdot \mathbf{b}_+ + \mathbf{U} \cdot \mathbf{b}_- \\ \mathbf{V} \cdot \mathbf{b}_+ + \mathbf{W} \cdot \mathbf{b}_- \end{pmatrix}. \tag{17}$$

Equation (17) splits up the $4N \times 4N$ linear system into two smaller $2N \times 2N$ systems, but it is not yet an efficient enough way to solve the problem.

1. Evaluation of the Field $\mathbf{X}_+$ on the Upper Surface

With the aim of solving $\mathbf{Z} \cdot \mathbf{X} = \mathbf{b}$ in an efficient way, we note that we need only the unknown values $\mathbf{X}_+$ to compute the scattered field in the upper medium Ω_0, above S^+. Consequently, in Eq. (17), we need only to solve $\mathbf{X}_+ = \mathbf{T} \cdot \mathbf{b}_+ + \mathbf{U} \cdot \mathbf{b}_-$. And, since $\mathbf{b}_- = \mathbf{0}$ in Eq. (8), it is equivalent to solve, by using Eq. (16a),

$$\mathbf{X}_+ = \mathbf{T} \cdot \mathbf{b}_+ = [\mathbf{Z}^U - \mathbf{C}^U \cdot (\mathbf{Z}^L)^{-1} \cdot \mathbf{C}^L]^{-1} \cdot \mathbf{b}_+. \tag{18}$$

The above expression can be cast into the form

$$\begin{aligned} \mathbf{X}_+ &= [\mathbf{I} - (\mathbf{Z}^U)^{-1} \cdot \mathbf{C}^U \cdot (\mathbf{Z}^L)^{-1} \cdot \mathbf{C}^L]^{-1} \cdot (\mathbf{Z}^U)^{-1} \cdot \mathbf{b}_+ \\ &= (\mathbf{I} - \mathbf{M}_c)^{-1} \cdot (\mathbf{Z}^U)^{-1} \cdot \mathbf{b}_+, \end{aligned} \tag{19}$$

where a characteristic matrix of the layer appears, which we name $\mathbf{M}_c$:

$$\mathbf{M}_c = (\mathbf{Z}^U)^{-1} \cdot \mathbf{C}^U \cdot (\mathbf{Z}^L)^{-1} \cdot \mathbf{C}^L. \tag{20}$$

If we define the norm $\|\cdot\|_{sr}$ of a complex matrix by its spectral radius, i.e., the highest modulus of its eigenvalues, we can expand the term $(\mathbf{I} - \mathbf{M}_c)^{-1}$ in Eq. (19), provided that

$$\|\mathbf{M}_c\|_{sr} = \|(\mathbf{Z}^U)^{-1} \cdot \mathbf{C}^U \cdot (\mathbf{Z}^L)^{-1} \cdot \mathbf{C}^L\|_{sr} < 1 \tag{21}$$

in the same way as the scalar expansion $1/(1-a) \simeq 1 + a + a^2 + a^3 + \cdots$ if $|a| < 1$. We will investigate in Subsection 3.D the validity domain of this condition, but we can already say that it is fulfilled for most configurations met in the literature.

Hence, when relation (21) is satisfied, expression (19) of the unknowns on the surface S^+ can be approximated by

$$\mathbf{X}_+^{(P)} = \left(\sum_{p=0}^{P} \mathbf{M}_c^p \right) \cdot (\mathbf{Z}^U)^{-1} \cdot \mathbf{b}_+ = \sum_{p=0}^{P} \mathbf{Y}_+^{(p)}, \tag{22}$$

where

$$\mathbf{Y}_+^{(0)} = (\mathbf{Z}^U)^{-1} \cdot \mathbf{b}_+, \qquad \mathbf{Y}_+^{(p)} = \mathbf{M}_c \cdot \mathbf{Y}_+^{(p-1)} \qquad \text{for } p > 0. \tag{23}$$

According to the expression of $\mathbf{M}_c$ given in Eq. (20), Eq. (22) has a clear physical interpretation (Fig. 2): The total unknowns on the upper interface are the sum of the contributions $\mathbf{Y}_+^{(p)}$ corresponding to successive iterations p. In the zeroth-order term, $(\mathbf{Z}^U)^{-1}$ accounts for the local interactions on the upper interface, so $\mathbf{Y}_+^{(0)}$ corresponds to the contribution of the direct reflection on the upper surface, without entering inside the layer. In the first-order term, given by $\mathbf{Y}_+^{(1)} = \mathbf{M}_c \cdot \mathbf{Y}_+^{(0)}$, $\mathbf{C}^L$ propagates the resulting upper field information, $\mathbf{Y}_+^{(0)}$, toward the lower interface, $(\mathbf{Z}^L)^{-1}$ accounts for the local interactions on the lower interface, and $\mathbf{C}^U$ repropagates the resulting contribution toward the upper interface; finally, $(\mathbf{Z}^U)^{-1}$ updates the field values on the upper interface. And so on for the subsequent terms $\mathbf{Y}_+^{(p)}$ for $p > 1$. The total field $\mathbf{X}_+^{(P)}$ on the upper interface corresponds to the multiple scattering of the field inside the layer. Furthermore, sum (22) converges to the exact and rigorous solution if relation (21) is fulfilled, because of the properties of the series expansion.

Taking into consideration this physical interpretation, we call our method PILE, for propagation-inside-layer expansion.

2. Evaluation of the Field $\mathbf{X}_-$ on the Lower Surface

The field $\mathbf{X}_-$ on the lower surface is computed from Eq. (17), with $\mathbf{b}_- = \mathbf{0}$, by using Eqs. (16c) and (18):

$$\mathbf{X}_- = \mathbf{V} \cdot \mathbf{b}_+ = -[(\mathbf{Z}^L)^{-1} \cdot \mathbf{C}^L] \cdot \mathbf{T} \cdot \mathbf{b}_+ = -[(\mathbf{Z}^L)^{-1} \cdot \mathbf{C}^L] \cdot \mathbf{X}_+. \tag{24}$$

Equation (24) can also be interpreted with the use of Fig. 2: From solution $\mathbf{X}_+$, obtained by exact inversion or iteratively (Subsection 3.A.1), $\mathbf{C}^L$ propagates the information toward the lower interface, then $(\mathbf{Z}^L)^{-1}$ accounts for the local interactions on this lower interface.

B. Use of Fast Methods Developed for Single Surfaces

The advantage of the PILE method [Eq. (22)] is that the matrix–vector products $(\mathbf{Z}^U)^{-1} \cdot \mathbf{v}$ and $(\mathbf{Z}^L)^{-1} \cdot \mathbf{v}$ (where $\mathbf{v}$ is

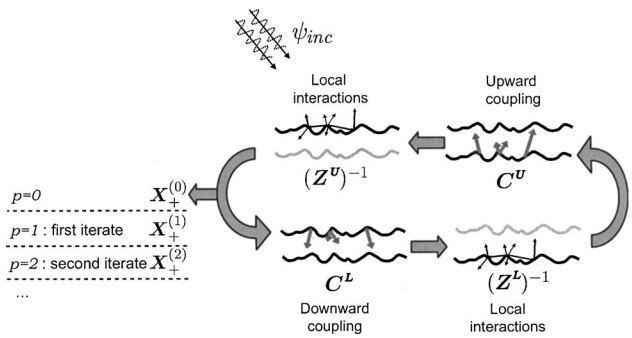

Fig. 2. Physical interpretation of $[(\mathbf{Z}^U)^{-1} \cdot \mathbf{C}^U \cdot (\mathbf{Z}^L)^{-1} \cdot \mathbf{C}^L]^p \cdot (\mathbf{Z}^U)^{-1}$.

a vector) can be calculated by fast numerical methods that already exist for a single rough interface.

Direct methods such as LU decomposition require $O(N^3/3)$ operations. As N increases, the computing cost becomes prohibitive. This has led to the development of iterative schemes that compute the surface unknowns in several steps. Three of the most extensively used approaches are the forward/backward (FB) method[25–28] (similar to the method of ordered multiple interactions[29]), the banded matrix iterative approach/canonical grid (BMIA/CAG),[23,30,31] and the fast multipole method (FMM).[32–34] Although any of these methods can be equally implemented for matrix inversion in the PILE method, we choose to use the BMIA/CAG because it is easier to implement than the FMM multilevel method and is more efficient than the existing version of the FB method for the dielectric case.[28]

In the BMIA/CAG method, the interaction between two points on the surface is split into near (strong) and far (weak) interactions. Near interactions are computed with the exact Green's function. In contrast, far interactions are computed by a Fourier transform through a Taylor series expansion of Green's function upon a flat surface ($z=0$). Therefore, the BMIA/CAG method is valid only for surfaces of up to a moderate roughness. A multilevel version of the BMIA/CAG has to be implemented for higher roughness; an alternative algorithm is the multigrid method.[35]

C. Complexity

The zeroth-order term $\mathbf{Y}_+^{(0)}=(\mathbf{Z}^U)^{-1}\cdot\mathbf{b}_+$ is obtained by applying a fast method (Subsection 3.B). With the use of the BMIA/CAG, this step has a complexity of $O(2N\log 2N)$, since $(\mathbf{Z}^U)^{-1}$ is of size $2N\times 2N$. The complexity per iteration of the terms $\mathbf{Y}_+^{(p)}$, $p>0$, is given below, with $\mathbf{v}=\mathbf{Y}_+^{(p-1)}$:

$$\mathbf{M}_c\cdot\mathbf{v}=(\mathbf{Z}^U)^{-1}\cdot\mathbf{C}^U\cdot(\mathbf{Z}^L)^{-1}\cdot\underbrace{\mathbf{C}^L\cdot\mathbf{v}}_{O(2N^2)\ \text{(a)}}\Big\}_{O(2N\log 2N)\ \text{(b)}}\Big\}_{O(2N^2)\ \text{(c)}}\Big\}_{O(2N\log 2N)\ \text{(d)}} \tag{25}$$

Operations (a) and (c) are matrix–vector multiplications: Their complexity is less than $O((2N)^2)$ because the $\mathbf{C}^U$ and $\mathbf{C}^L$ matrices are mid empty. Operations (b) and (d) are fast iterative inversions, computed with the BMIA/CAG or with any other fast method. In conclusion, this method is of order $O(4PN^2+(1+2P)2N\log 2N)$, where P is the number of iterations, i.e., the truncation order in series expansion (22). For $N\gg 1$, we get $O(4PN^2)$. As we can see from the numerical results, P is generally less than 10, so this method is much faster than the direct LU inversion, of order $O((4N/3)^3)$. Furthermore, the PILE method is faster than a conjugate gradient scheme, whose complexity is $O(M_{iter}12N^2)$, where M_{iter} is the number of iterations and $12N^2$ is the number of nonzero coefficients of the impedance matrix.

In the same way, for the perfectly conducting case, the complexity of the PILE method at order P is $O(3PN^2+N[(3P+2)\log N+2(P+1)\log 2])$. When $N\gg 1$, this leads to a complexity of $O(3PN^2)$.

D. Validity Domain

The convergence of the PILE method relies on condition (21) on $\mathbf{M}_c$, involving the four submatrices of the impedance matrix of the layer in Eq. (9), which depend on the parameters of the system: statistics of the interfaces, mean thickness of the layer, and permittivity of each medium. Nevertheless, it is worth noting that the norm is independent of the incident angle. We study hereafter the following configurations: (a) two plane interfaces, (b) one rough interface above or under a plane interface, and (c) two rough interfaces. In each case, a typical relative dielectric permittivity of the layer is chosen, $\varepsilon_{r1}=2.5+0.01i$, as in Refs. 22 and 36–39.

1. Influence of the Layer Thickness: Case (a)

For a relative dielectric permittivity of lower medium Ω_2 chosen as $\varepsilon_{r2}=8$, the Green's function g_2 in Ω_2 varies faster than the Green's function g_0 in free space Ω_0. Actually, the number of sampling points needed in Ω_2 should be $\sqrt{8}\simeq 3$ times higher than that in free space. As ten sampling points per wavelength are usually taken in free space, we choose therefore 30 sampling points per wavelength for each interface, so $\Delta x\simeq 0.03\lambda$. We plot in Fig. 3 the norm $\|\mathbf{M}_c\|_{sr}$ versus the thickness H of the layer, for several values $L/\lambda=\{6,9,12,15\}$ of the total length of each interface, for TE (top) and TM (bottom) polarizations. The lower limit value of the thickness, $H=0.03\lambda$, is equal to Δx. We note that the norm is higher in TE polarization than in TM polarization. In addition, the norm increases when the thickness decreases, as a consequence of a higher coupling between the two interfaces. Nevertheless, the method converges for both polarizations, for whatever thickness greater than Δx, for the considered lengths. In addition, for a given thickness, the norm increases if the length L increases. Considering next the perfectly conducting case, we plot in Fig. 4 the norm versus the thickness H, with the same parameters as those in Fig. 3, except for $\varepsilon_{r2}=i\infty$. Results are quite similar for both polarizations, unlike for the dielectric case. But above all, it is worth noting that the norm is higher than that for the dielectric case; this implies that the PILE method converges more quickly for the dielectric case than for the perfectly conducting one.

2. Influence of the Roughness: Cases (b) and (c)

Let us consider rough interfaces with both Gaussian height distribution and correlation. We first study the case of one rough interface above or under a plane interface [case (b)] for the dielectric case.

We plot in Fig. 5 the norm $\|\mathbf{M}_c\|_{sr}$ versus the height rms σ_h of the rough interface. For each interface, the total length is $L=12\lambda$, the sampling rate is $\Delta x=0.03\lambda$, and the number of samples is $N=400$; the correlation length is equal to $L_c=\lambda$. The slope rms is then given by $\sigma_p=\sqrt{2}\sigma_h/L_c=\sqrt{2}\sigma_h/\lambda$. The mean thickness is $H=1.5\lambda$. Other parameters, such as dielectric constants, are identical to those in the plane case (Fig. 3). The upper limit for height

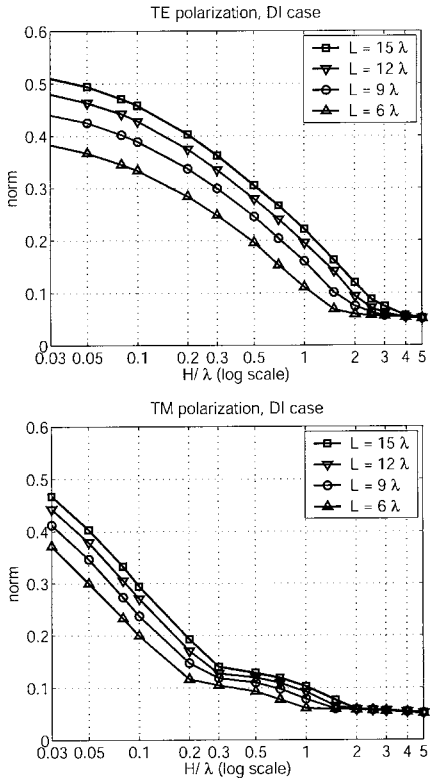

Fig. 3. Norm $\|\mathbf{M}_c\|_{sr}$ versus thickness H for the dielectric (DI) case: TE (top) and TM (bottom) polarizations, two plane surfaces, $\Delta x=0.03\lambda$, $\varepsilon_{r0}=1$, $\varepsilon_{r1}=2.5+0.01i$, and $\varepsilon_{r2}=8$.

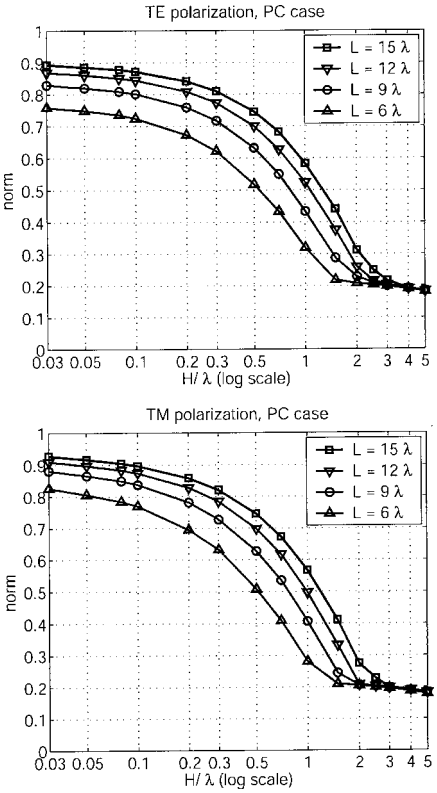

Fig. 4. Norm $\|\mathbf{M}_c\|_{sr}$ versus thickness H for the perfectly conducting (PC) case: TE (top) and TM (bottom) polarizations, two plane surfaces, $\Delta x=0.03\lambda$, $\varepsilon_{r0}=1$, $\varepsilon_{r1}=2.5+0.01i$, and $\varepsilon_{r2}=i\infty$.

rms is chosen as $\sigma_{h,max}=0.3\lambda=H/5$, so that the rough surface does not intercept the plane surface. We can note in Fig. 5 (i.e., for $\sigma_h\leqslant 0.3\lambda$ and $\sigma_p\leqslant\sqrt{2}\times 0.3\simeq 0.42$) that the difference between the norm in the case of a single rough surface, above or under a plane one, and the norm in the plane case ($\sigma_h=0$) is less than ±0.05. In other words, a moderate roughness does not modify drastically the norm of the characteristic matrix of the layer.

When both surfaces are rough [case (c)], several cases arise: Surfaces can be uncorrelated between themselves, correlated, or identical. Further investigations, not shown here, point out that the norm is not modified in a significant way (same range of ±0.05), whatever the correlation between surfaces and the height rms. This behavior of the norm is illustrated, for example, in Fig. 6, where we plot the norm versus σ_h for the case of identical or uncorrelated rough surfaces. In this example, we choose an identical height rms for both surfaces, $\sigma_h=\sigma_h^+=\sigma_h^-$. Other parameters are the same as those in Fig. 5 ($L_c=\lambda$, $L=12\lambda$, $\Delta x=0.03\lambda$, $N=400$, and $H=1.5\lambda$).

For the perfectly conducting case also, results, not shown here, confirm that the roughness has a similar low influence on the norm.

3. Influence of the Total Length L

If we consider moderate roughness up to $\sigma_h\simeq 0.3\lambda$, the norm of the characteristic matrix is mostly influenced by

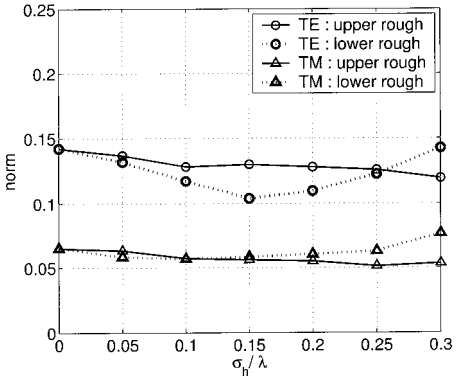

Fig. 5. Norm $\|\mathbf{M}_c\|_{sr}$ versus height rms σ_h for one rough surface and one plane surface: upper rough (solid curves) or lower rough (dashed curves), dielectric case for both polarizations, $H=1.5\lambda$, $L=12\lambda$, $\Delta x=0.03\lambda$, $\varepsilon_{r0}=1$, $\varepsilon_{r1}=2.5+0.01i$, and $\varepsilon_{r2}=8$.

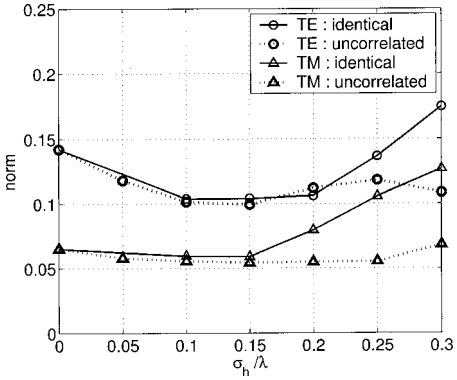

Fig. 6. Norm $\|\mathbf{M}_c\|_{sr}$ versus height rms σ_h for both rough surfaces: identical surfaces (solid curves) or uncorrelated surfaces (dashed curves), dielectric case for both polarizations, $H=1.5\lambda$, $L=12\lambda$, $\Delta x=0.03\lambda$, $\varepsilon_{r0}=1$, $\varepsilon_{r1}=2.5+0.01i$, and $\varepsilon_{r2}=8$.

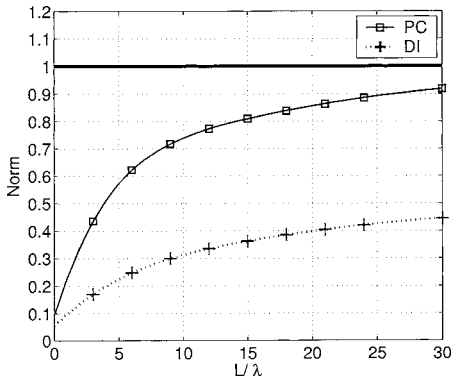

Fig. 7. Norm $\|\mathbf{M}_c\|_{sr}$ versus total length L for perfectly conducting and dielectric cases: TE polarization, $H=0.3\lambda$ and $\Delta x=0.03\lambda$ for both plane surfaces.

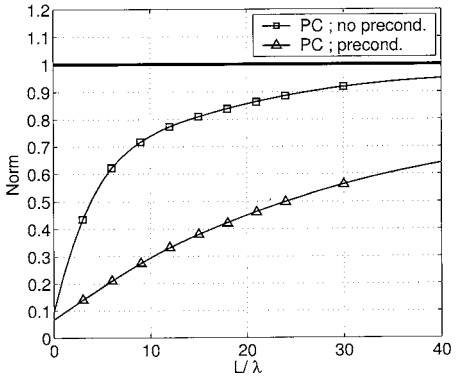

Fig. 8. Influence of preconditioning: norm $\|\mathbf{M}_c\|_{sr}$ versus total length L (squares) and norm $\|(\mathbf{I}-\mathbf{M}_0)^{-1}(\mathbf{M}_c-\mathbf{M}_0)\|_{sr}$ with $b=51$ (triangles), for the perfectly conducting case and TE polarization for both plane surfaces.

the total length L of the surfaces and the mean thickness H of the layer. In Figs. 3 and 4, we plotted the norm versus the thickness H for a given L; let us consider now (Fig. 7) the influence of the total length L on the norm for a given thickness H. We study how the PILE method converges, even for a small thickness ($H=0.3\lambda$). Figure 7 illustrates results for TE polarization only, the TM case being very similar. The maximal value $L=30\lambda$ corresponds to the maximal size that we can solve by direct inversion on our computer ($N=1000$ sampling points for each surface).

Figures 3, 4, and 7 show that the norm is higher for the perfectly conducting case than for the dielectric case. But the relevant point is that the increase of the norm is slowing down for increasing values of L. Hence, we can expect that the norm will be less than unity, i.e., the PILE method will converge, for L values up to 200λ in the dielectric case.

E. Preconditioning

A way to improve and, consequently, to accelerate the convergence of the PILE method is to precondition the characteristic matrix of the layer, $\mathbf{M}_c$, by reducing its norm (21). Another point is that errors over successive iterates $\mathbf{Y}_+^{(p)}$ propagate by applying recursively $\mathbf{M}_c$; hence, a reduction of its norm can reduce the final error of the PILE method.

In Eq. (19), we intend to expand $(\mathbf{I}-\mathbf{M}_c)^{-1}$ in a series more quickly convergent than $\mathbf{I}+\mathbf{M}_c+\mathbf{M}_c^2+\mathbf{M}_c^3+\cdots$. For this purpose, let us suppose that a matrix $\mathbf{M}_0$ exists, which is close to $\mathbf{M}_c$ and such that $(\mathbf{I}-\mathbf{M}_0)^{-1}$ is easier to invert than $(\mathbf{I}-\mathbf{M}_c)^{-1}$, i.e., with fewer operations. Then

$$\begin{aligned}(\mathbf{I}-\mathbf{M}_c)^{-1} &= [\mathbf{I}-\mathbf{M}_0-(\mathbf{M}_c-\mathbf{M}_0)]^{-1}\\ &= \{(\mathbf{I}-\mathbf{M}_0)[\mathbf{I}-(\mathbf{I}-\mathbf{M}_0)^{-1}(\mathbf{M}_c-\mathbf{M}_0)]\}^{-1}\\ &= [\mathbf{I}-(\mathbf{I}-\mathbf{M}_0)^{-1}(\mathbf{M}_c-\mathbf{M}_0)]^{-1}(\mathbf{I}-\mathbf{M}_0)^{-1}.\end{aligned} \tag{26}$$

The expression $[\mathbf{I}-(\mathbf{I}-\mathbf{M}_0)^{-1}(\mathbf{M}_c-\mathbf{M}_0)]^{-1}$ can be expanded in a series as in Eq. (22) if

$$\|(\mathbf{I}-\mathbf{M}_0)^{-1}(\mathbf{M}_c-\mathbf{M}_0)\|_{sr}<1. \tag{27}$$

It is interesting to note that an appropriate choice of $\mathbf{M}_0$ may lead to

$$\|(\mathbf{I}-\mathbf{M}_0)^{-1}(\mathbf{M}_c-\mathbf{M}_0)\|_{sr}<\|\mathbf{M}_c\|_{sr}<1. \tag{28}$$

The efficiency of preconditioning relies on the choice of $\mathbf{M}_0$. More precisely, we search for a matrix $\mathbf{M}_0$ that has eigenvalues "close" to those of $\mathbf{M}_c$ and that is easy to invert. Hence, we choose $\mathbf{M}_0=(\mathbf{Z}_B^U)^{-1}\cdot\mathbf{C}_B^U\cdot(\mathbf{Z}_B^L)^{-1}\cdot\mathbf{C}_B^L$, where the subscript B stands for the corresponding banded matrices of four matrices of $\mathbf{M}_c$, given in Eqs. (10) and (11). These banded block matrices have a size of $N\times N$ and equal band width b. Therefore, $\mathbf{M}_0$ is also a banded matrix, and we can then proceed to the approximate computation of $(\mathbf{I}-\mathbf{M}_0)^{-1}$ by incomplete LU matrix factorization,[38] which is a low-cost operation.

Finally, the preconditioned PILE method has a similar expression to Eq. (22):

$$\mathbf{X}_+^{(P)}=\left\{\sum_{p=0}^{P}[(\mathbf{I}-\mathbf{M}_0)^{-1}(\mathbf{M}_c-\mathbf{M}_0)]^p\right\}(\mathbf{I}-\mathbf{M}_0)^{-1}\cdot(\mathbf{Z}^U)^{-1}\cdot\mathbf{b}_+. \tag{29}$$

Figure 8 shows a comparison of the norm of the characteristic matrix with and without preconditioning. We consider TE polarization, both plane surfaces, and a perfectly conducting lower medium. The nonpreconditioned results are those of Fig. 7. For the preconditioning, we choose a bandwidth of $b=51$ coefficients, according to studies carried out in Ref. 19. Such a choice for b induces at the same time a low norm of the preconditioned matrix and a low bandwidth, i.e., a low-cost LUINC decomposition. We can note that preconditioning appreciably reduces the norm for this configuration: For instance, with a total length $L=30\lambda$, $\|\mathbf{M}_c\|_{sr}\simeq 0.92$ whereas $\|(\mathbf{I}-\mathbf{M}_0)^{-1}(\mathbf{M}_c-\mathbf{M}_0)\|_{sr}\simeq 0.57$.

4. VALIDATION OF THE PROPAGATION-INSIDE-LAYER EXPANSION METHOD

The PILE method is compared with two results from the literature.[22,39]

A. Sand Layer on a Granite Surface

As a first example, we compare results obtained by the PILE method and by another rigorous integral method,[22] which was first applied to a single dielectric rough

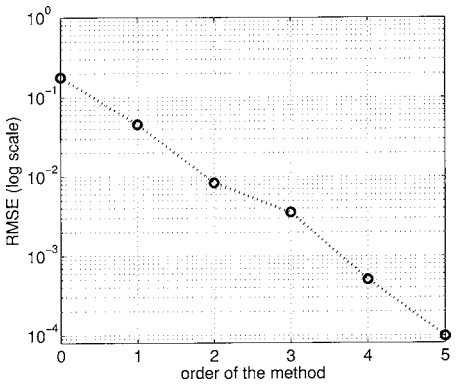

Fig. 9. rms error for different orders P of the PILE method. The same parameters are used as those of Fig. 9 in Ref. 22: $\varepsilon_{r0}=1$, $\varepsilon_{r1}=2.5+0.01i$, and $\varepsilon_{r2}=8$. Parameters of rough surfaces are $L=70\lambda$, $\Delta x=0.03\lambda$, $\sigma_h^+=0.01\lambda$, $\sigma_p^+=0.014$, $\sigma_h^-=0.35\lambda$, $\sigma_p^+=0.49$, and $H=1.5\lambda$, and TE polarization is used. Parameters of the Thorsos tapered incident wave are $\theta_i=30°$ and $g=L/6\simeq 11.7\lambda$.

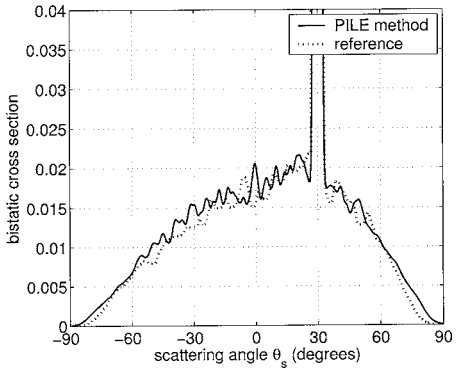

Fig. 10. Bistatic cross section in TE polarization. The dashed curve is the result of Fig. 9 in Ref. 22, and the solid curve represents the PILE method at order 5.

surface.[40] For a stack of two rough surfaces, both the PILE method and this alternative integral method allow one to deal with a reduced number of unknowns ($2N$ instead of $4N$ for the dielectric case and $3N$ for the perfectly conducting case). However, the main difference is that the impedance matrix of Ref. 22 is arranged in a compact form, inducing a more complicated formulation of the kernel of the operator. Hence, the fill-in of the impedance matrix is very time-consuming, and, furthermore, the complicated formulation makes it more difficult to develop fast methods of resolution. In addition, Saillard and Toso[22] use the beam simulation method,[41] with incident Gaussian waves, whereas we use the Thorsos tapered waves.[21]

First we study the configuration (Fig. 9 of Ref. 22) modeling a flat-top sand layer superimposed on a rough granite surface. This configuration deals with two surfaces of very different roughnesses: The upper, air–sand interface fulfills the conditions of application of the small-perturbation method (height rms $\sigma_h^+=0.01\lambda$, slope rms $\sigma_p^+=0.014$), whereas the lower, sand–granite interface fulfills the Kirchhoff approximation ($\sigma_h^-=0.35\lambda$, $\sigma_p^+=0.49$). The two surfaces are assumed to be uncorrelated between themselves.

We choose a Thorsos incident tapered wave with a tapering parameter $g=L/6\simeq 11.7\lambda$, where the total length is $L=70\lambda$. The other parameters are incident angle $\theta_i=30°$, $\varepsilon_{r0}=1$, $\varepsilon_{r1}=2.5+0.01i$, $\varepsilon_{r2}=8$, mean thickness $H=1.5\lambda$, and $N=2300$ sampling points for each interface. The scattering patterns are averaged over 300 realizations by means of a Monte Carlo procedure.

To quantify the convergence of the PILE method for this configuration, we realize an exact LU inversion of the impedance matrix with expressions (16). Next we compute the bistatic cross section (BCS) rms error of the PILE method at order P versus the exact inversion. In Fig. 9 of this paper, this rms error decreases rapidly as the order of the PILE method increases: A rms error of 1% is obtained at order 2, and 0.01% is reached at order 5. In Fig. 10, we plot the BCS in a linear scale for TE polarization; reference results are those given in Ref. 22, and the

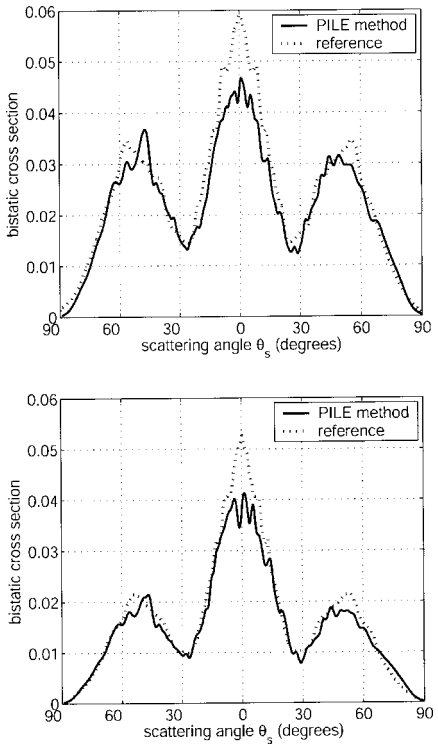

Fig. 11. Bistatic cross section in TE (top) and TM (bottom) polarizations. The dashed curves are the result of Fig. 11 in Ref. 22, and the solid curves represent the PILE method at order 5.

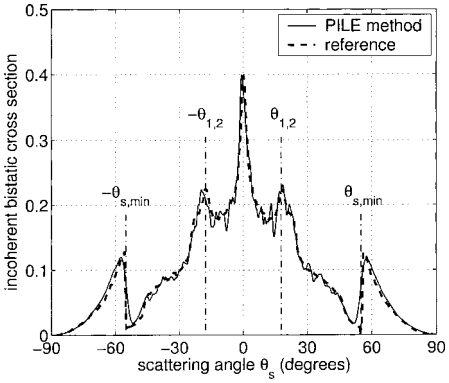

Fig. 12. *Incoherent* bistatic cross section in TE polarization. The dashed curve is the result of Fig. 3 in Ref. 39, and the solid curve represents the PILE method at order 15.

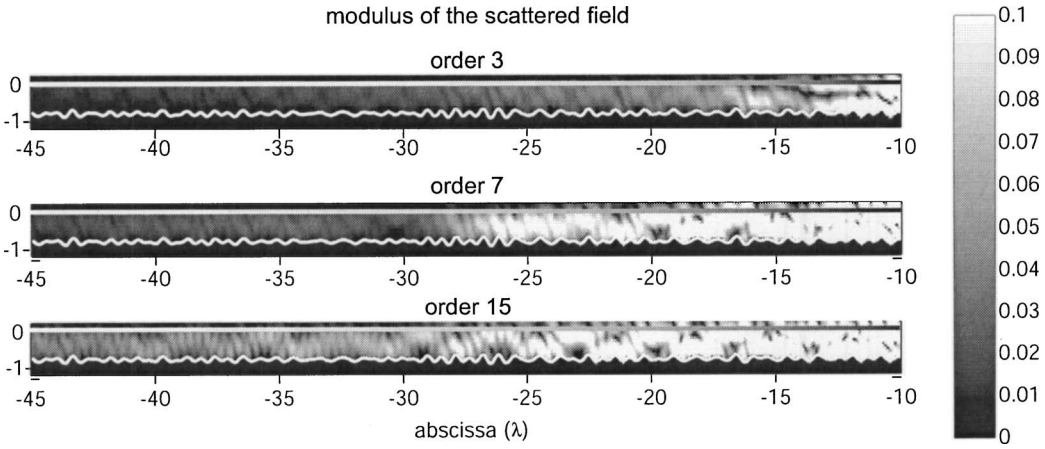

Fig. 13. Comparison of the modulus of the field inside the layer for different orders of the PILE method. The parameters are the same as those in Fig. 12.

PILE results are computed up to order 5. According to Fig. 10, results of both rigorous integral methods are in good agreement.

Second, we study the configuration of Fig. 11 of Ref. 22. The parameters are the same as those in Fig. 10, except that $\theta_i = 0°$ and the upper surface is now identical to the lower one ($\sigma_h^{\pm} = 0.35\lambda$, $\sigma_p^{\pm} = 0.49$). Results are plotted in Fig. 11 of this paper for both polarizations; the BCSs are in good agreement, except for the normal scattering direction. These differences can be explained by the different choices of incident beams.

B. Layer with Rough Lower Interface of the West–O'Donnell Spectrum

We now focus on the configuration in Fig. 3 of Ref. 39. The incident Thorsos beam ($\lambda = 633$ nm, $g = L/10 = 16\lambda$, with $L = 160\lambda$) is normally incident ($\theta_i = 0°$). The upper surface is a plane, whereas the lower one is characterized by a Gaussian surface height distribution ($\sigma_h^- = 30$ nm $\simeq 0.047\lambda$) and by a West–O'Donnell power spectrum,[20] defined by the parameters $k_{low} = 0.82k_0$ and $k_{up} = 1.97k_0$, where k_0 is the wave number in air. The relative dielectric permittivity of the layer is $\varepsilon_{r1} = 2.69 + 0.01i$, and the lower medium is assumed to be perfectly conducting. The mean thickness of the layer is $H = 500$ nm $\simeq 0.79\lambda$.

To derive the scattered field, Simonsen and Maradudin[39] use an asymptotic model, based on reduced Rayleigh equations, and they average the incoherent BCS with a Monte Carlo procedure.

Figure 12 shows the incoherent BCS provided by this asymptotic method, denoted as the reference method, and by our rigorous PILE method at order 15. We plot here only results for TE polarization, the TM ones being similar. We apply the MoM with $N = 3200$ sampling points, so we deal with 9600 unknowns. Our results (solid curve), averaged over 300 surface realizations, are in very good agreement with reference ones (dashed curve), resulting from 3000 realizations.

Some physical comments can be made about the incoherent BCS. First, as the lower surface is of the West–O'Donnell kind, single-scattering processes contribute to the BCS only in directions θ_s such that $|\theta_s| > \theta_{s,min}$, where $|k_0 \sin \theta_{s,min}| = k_{low}$. We find[39] that $\theta_{s,min} \simeq 55.1°$. This phenomenon produces an abrupt increase of the BCS for angles $|\theta_s| > 55°$ in Fig. 12. Second, in the absence of roughness and absorption, the layer can support guided waves: In TE polarization, only two modes exist, with wave numbers $q_1 = 1.24k_0$ and $q_2 = 1.55k_0$.[36] The beat yielded by these two close guided modes creates[36] two satellite peaks in the BCS for angles $\theta_{(1,2)}^{\pm}$ such as $\sin \theta_{(1,2)}^{\pm} = -\sin \theta_i \pm (1/k_0)(q_1 - q_2)$. The theoretical value $\theta_{(1,2)}^{\pm} \simeq \pm 17.7°$ is in good agreement with observations from Fig. 12.

It is interesting to note that parameters k_{low} and k_{up} of the West–O'Donnell lower surface satisfy $k_{low} < q_1 < q_2 < k_{up}$ and, therefore, permit a strong excitation of guided modes inside the layer.

Furthermore, the PILE method permits the enlightenment of physical phenomena inside the layer. From solutions $\mathbf{X}_+^{(P)}$ and $\mathbf{X}_-^{(P)}$ calculated on both surfaces [Eqs. (14), (22), and (24)], we can calculate the scattered field inside the layer (Subsection 2.D). Figure 13 presents the modulus of this scattered field, obtained from the solutions at orders $P = \{3, 7, 15\}$. This figure confirms that the different orders of the PILE method take into account the successive multiple reflections inside the layer. The beat yielded by the two close guided modes, with wave numbers q_1 and q_2, is clearly seen, particularly in the solution of order 15. These guided modes induce a slow decay of the field and, consequently, a slower convergence of the PILE method (15 orders) for this later configuration than in Subsection 4.A (only 5 orders). Nevertheless, if we apply the preconditioned formulation given by Eq. (29), the number of iterations required to achieve the same precision drops from 15 to 8.

C. CPU Requirements

We used $N = 2300$ sampling points (9200 unknowns) for the configuration of Figs. 10 and 11 and $N = 3200$ sampling points (9600 unknowns) for Fig. 12. The size of the impedance matrix $\mathbf{Z}$ of the layer is then about 1.5 Gbits. It is worth noting that, even for such a high number of unknowns, calculations are tractable with the PILE method on a standard personal computer (2 GHz processor, 1 Gbit RAM) with MATLAB; the typical CPU time for this number of samples is about

- 8 min per realization at order 5 (Figs. 10 and 11),
- 30 min per realization at order 15 (Fig. 12).

Moreover, we cannot provide comparisons with the LU method of inversion, because it is impossible to carry out calculations with such a big impedance matrix.

5. CONCLUSION

In this paper, we have considered integral methods to solve the problem of electromagnetic scattering by one-dimensional rough layers. The integral equations and the corresponding linear system have been introduced, as well as physical insights into the blocks of the impedance matrix. Although these equations have been known for almost 15 years,[17] no efficient method of resolution had been developed until now.

We have presented herein such a fast method to study the electromagnetic scattering by a one-dimensional rough layer; to our knowledge, the propagation-inside-layer expansion (PILE) method is the first efficient method devoted to this configuration. Its main interest is that it is rigorous, with a simple formulation and with a straightforward physical interpretation. Actually, this last property relies on the fact that each block of the impedance matrix is linked to a particular and quasi-independent physical process occurring during the multiple-scattering process inside the layer: Local scattering on each interface and both upward and downward coupling. By the way, this ensures that, in its validity domain, the method converges fast (commonly in 5–10 iterations), even without preconditioning.

Furthermore, the PILE method allows one to use any fast method developed for a single interface. The BMIA/CAG method has been implemented in the present case, but any other method, such as the FB method or FMM, could be used instead.

Another advantage is that it is the first method able to deal with problems with a huge number of unknowns, as for instance those involving high incident angles or guided waves. Finally, the quite large validity domain of the PILE method makes it able to handle most of the configurations studied in the literature and allows us to study new ones, in particular without restrictions to small roughness. The only limitation is the low convergence of the method when dealing with very thin layers.

Further investigations could be directed toward implementing the PILE method to the case of a target located below a rough surface[42]; indeed, the equations in this case are very similar to those of the rough layer case.

APPENDIX A: IMPEDANCE MATRIX COEFFICIENTS

For the dielectric case, the matrices $\mathbf{A}^+$, $\mathbf{B}^+$, $\mathbf{C}^+$, $\mathbf{D}^+$, $\mathbf{E}$, $\mathbf{F}$, $\mathbf{G}$, and $\mathbf{H}$ of the impedance matrix $\mathbf{Z}$ have the following expressions:

$$A^+_{mn}=\begin{cases} -\dfrac{i\Delta x k_0}{4}\dfrac{H_1^{(1)}(k_0\|\mathbf{r}_n^+-\mathbf{r}_m^+\|)}{\|\mathbf{r}_n^+-\mathbf{r}_m^+\|} \\ \times\{\zeta^{+\prime}(x_n)(x_n-x_m)-[\zeta^+(x_n)-\zeta^+(x_m)]\} & \text{for } m\neq n \\ +\dfrac{1}{2}-\dfrac{\Delta x}{4\pi}\dfrac{\zeta^{+\prime\prime}(x_m)}{1+(\zeta^{+\prime}(x_m))^2} & \text{for } m=n \end{cases}, \quad \text{(A1)}$$

$$B^+_{mn}=\begin{cases} \gamma_n^+\dfrac{i\Delta x}{4}H_0^{(1)}(k_0\|\mathbf{r}_n^+-\mathbf{r}_m^+\|) & \text{for } m\neq n \\ \gamma_n^+\dfrac{i\Delta x}{4}\left[1+i\dfrac{2}{\pi}\log\left(\dfrac{e^\gamma}{2}\dfrac{k_0\Delta x}{2e}\gamma_n^+\right)\right] & \text{for } m=n \end{cases}, \quad \text{(A2)}$$

$$C^+_{mn}=\begin{cases} -\dfrac{i\Delta x k_1}{4}\dfrac{H_1^{(1)}(k_1\|\mathbf{r}_n^+-\mathbf{r}_m^+\|)}{\|\mathbf{r}_n^+-\mathbf{r}_m^+\|} \\ \times\{\zeta^{+\prime}(x_n)(x_n-x_m)-[\zeta^+(x_n)-\zeta^+(x_m)]\} & \text{for } m\neq n \\ -\dfrac{1}{2}-\dfrac{\Delta x}{4\pi}\dfrac{\zeta^{+\prime\prime}(x_m)}{1+(\zeta^{+\prime}(x_m))^2} & \text{for } m=n \end{cases}, \quad \text{(A3)}$$

$$D^+_{mn}=\begin{cases} \gamma_n^+\dfrac{i\Delta x}{4}H_0^{(1)}(k_1\|\mathbf{r}_n^+-\mathbf{r}_m^+\|) & \text{for } m\neq n \\ \gamma_n^+\dfrac{i\Delta x}{4}\left[1+i\dfrac{2}{\pi}\log\left(\dfrac{e^\gamma}{2}\dfrac{k_1\Delta x}{2e}\gamma_n^+\right)\right] & \text{for } m=n \end{cases}, \quad \text{(A4)}$$

$$E_{mn}=+\frac{i\Delta x k_1}{4}\frac{H_1^{(1)}(k_1\|\mathbf{r}_n^--\mathbf{r}_m^+\|)}{\|\mathbf{r}_n^--\mathbf{r}_m^+\|} \times\{\zeta^{-\prime}(x_n)(x_n-x_m)-[\zeta^-(x_n)-\zeta^+(x_m)]\} \qquad \forall\, m,n, \quad \text{(A5)}$$

$$F_{mn}=-\gamma_n^-\frac{i\Delta x}{4}H_0^{(1)}(k_1\|\mathbf{r}_m^+-\mathbf{r}_n^-\|) \qquad \forall\, m,n, \quad \text{(A6)}$$

$$G_{mn}=+\frac{i\Delta x k_1}{4}\frac{H_1^{(1)}(k_1\|\mathbf{r}_n^+-\mathbf{r}_m^-\|)}{\|\mathbf{r}_n^+-\mathbf{r}_m^-\|} \times\{\zeta^{+\prime}(x_n)(x_n-x_m)-[\zeta^+(x_n)-\zeta^-(x_m)]\} \qquad \forall\, m,n, \quad \text{(A7)}$$

$$H_{mn}=-\gamma_n^+\frac{i\Delta x}{4}H_0^{(1)}(k_1\|\mathbf{r}_m^--\mathbf{r}_n^+\|) \qquad \forall\, m,n, \quad \text{(A8)}$$

where $\|\mathbf{r}_n^\pm-\mathbf{r}_m^\pm\|=\sqrt{(x_n-x_m)^2-(\zeta^\pm(x_n)-\zeta^\pm(x_m))^2}$, $\gamma_n^\pm=\sqrt{1+(\zeta^{\pm\prime}(x_n))^2}$, and $\gamma\simeq 0.5772$ is Euler's constant.

$\mathbf{A}^-$, $\mathbf{B}^-$, $\mathbf{C}^-$, and $\mathbf{D}^-$ are very similar to $\mathbf{A}^+$, $\mathbf{B}^+$, $\mathbf{C}^+$, and $\mathbf{D}^+$, respectively, where $\mathbf{r}^+_{\{m,n\}}$ is replaced by $\mathbf{r}^-_{\{m,n\}}$, γ_n^+ by γ_n^-, ζ^+ by ζ^-, k_0 by k_1, and k_1 by k_2. These expressions can also be used in the perfectly conducting case (Subsection 2.C).

The authors may be reached at the following e-mail addresses: ndechamps@chem-eng.utoronto.ca, nicole.debeaucoudrey@univ-nantes.fr, christophe.bourlier@univ-nantes.fr, serge.toutain@univ-nantes.fr.

REFERENCES

1. C. Amra, G. Albrand, and P. Roche, "Theory and application of antiscattering single layers: antiscattering antireflection coatings," Appl. Opt. **16**, 2695–2702 (1986).
2. G. V. Rozhnov, "Electromagnetic wave diffraction by multilayer media with rough interface," Sov. Phys. JETP **69**, 646–651 (1989).
3. C. Amra, "Light scattering from multilayer optics. I. Tools of investigation," J. Opt. Soc. Am. A **11**, 197–210 (1994).
4. C. Amra, "Light scattering from multilayer optics. II. Application to experiment," J. Opt. Soc. Am. A **11**, 211–226 (1994).
5. I. Ohlidal and K. Navratil, "Scattering of light from multilayer systems with rough boundaries," Prog. Opt. **34**, 251–334 (1995).
6. H. Kaplan, "Black coatings are critical in optical design," Photonics Spectra **31**, 48–50 (1997).
7. R. Garcia-Llamas, L. E. Regalado, and C. Amra, "Scattering of light from a two-layer system with a rough surface," J. Opt. Soc. Am. A **16**, 2713–2719 (1999).
8. I. M. Fuks and A. G. Voronovich, "Wave diffraction by rough interfaces in an arbitrary plane-layered medium," Waves Random Media **10**, 253–272 (2000).
9. I. M. Fuks, "Wave diffraction by a rough boundary of an arbitrary plane-layered media," IEEE Trans. Antennas Propag. **49**, 630–639 (2001).
10. Z. Otremba and J. Piskozub, "Modelling of the optical contrast of an oil film on a sea surface," Opt. Express **9**, 411–416 (2001).
11. D. Goodman and Conyers, *Ground Penetrating Radar, An Introduction for Archaeologists* (Altamira, 1997).
12. T. M. Elfouhaily and C.-A. Guérin, "A critical survey of approximate scattering wave theories from random rough surfaces," Waves Random Media **14**, R1–R40 (2004).
13. M. Saillard and A. Sentenac, "Rigorous solution for electromagnetic scattering from rough surfaces," Waves Random Media **11**, R103–R137 (2001).
14. K. F. Warnick and W. C. Chew, "Numerical simulation methods for rough surface scattering: topical review," Waves Random Media **11**, R1–R30 (2001).
15. F. Harrington, *Field Computation by Moment Methods* (IEEE Press, 1993).
16. L. Tsang, J. A. Kong, K.-H. Ding, and C. O. Ao, *Scattering of Electromagnetics Waves: Numerical Simulations* (Wiley, 2001).
17. J. Q. Lu, A. A. Maradudin, and T. Michel, "Enhanced backscattering from a rough dielectric film on a reflecting substrate," J. Opt. Soc. Am. B **8**, 311–318 (1991).
18. V. Freilikher, E. Kanzieper, and A. A. Maradudin, "Coherent scattering enhancement in systems bounded by rough surfaces," Phys. Rep. **288**, 127–204 (1997).
19. N. Déchamps, "Numerical methods for electromagnetic wave scattering from one-dimensional rough surfaces," Ph.D. thesis (IREENA, Polytech'Nantes, Université de Nantes, 2004).
20. C. S. West and K. A. O'Donnell, "Observations of backscattering enhancement from polaritons on a rough metal surface," J. Opt. Soc. Am. A **12**, 390–397 (1995).
21. E. I. Thorsos, "The validity of the Kirchhoff approximation for rough surface scattering using a Gaussian roughness spectrum," J. Acoust. Soc. Am. **83**, 78–92 (1988).
22. M. Saillard and G. Toso, "Electromagnetic scattering from bounded or infinite subsurface bodies," Radio Sci. **32**, 1347–1359 (1997).
23. L. Tsang, C. H. Chan, K. Pak, and H. Sangani, "Monte-Carlo simulations of large-scale problems of random rough surface scattering and applications to grazing incidence with the BMIA/canonical grid method," IEEE Trans. Antennas Propag. **43**, 851–859 (1995).
24. W. H. Press, S. A. Teukolsky, W. T. Vetterling, and B. P. Flannery, *Numerical Recipes*, 2nd ed. (Cambridge U. Press, 1992).
25. D. Holliday, L. L. DeRaad, Jr., and G. J. St-Cyr, "Forward–backward: a new method for computing low-grazing angle scattering," IEEE Trans. Antennas Propag. **44**, 722–729 (1996).
26. D. Holliday, L. L. DeRaad, Jr., and G. J. St-Cyr, "Forward–backward method for scattering from imperfect conductors," IEEE Trans. Antennas Propag. **46**, 101–107 (1998).
27. H. T. Chou and J. T. Johnson, "A novel acceleration of scattering from rough surfaces with the forward–backward method," Radio Sci. **33**, 1277–1287 (1998).
28. A. Iodice, "Forward–backward method for scattering from dielectric rough surfaces," IEEE Trans. Antennas Propag. **50**, 901–911 (2002).
29. D. A. Kapp and G. S. Brown, "A new numerical method for rough-surface scattering calculations," IEEE Trans. Antennas Propag. **44**, 711–722 (1996).
30. L. Tsang, C. H. Chang, and H. Sangani, "A banded matrix iterative approach to Monte Carlo simulations of scattering of waves by large-scale random rough surface problems: TM case," Electron. Lett. **29**, 166–167 (1993).
31. Q. Li, C. H. Chan, and L. Tsang, "Monte-Carlo simulations of wave scattering from lossy dielectric random rough surfaces using the physics-based two-grid method and the canonical-grid method," IEEE Trans. Antennas Propag. **47**, 752–763 (1999).
32. V. Rokhlin, "Rapid solution of integral equations of scattering theory in two dimensions," J. Comput. Phys. **36**, 414–439 (1990).
33. N. Engheta, W. D. Murphy, V. Rokhlin, and M. S. Vassiliou, "The fast multipole method (FMM) for electromagnetic scattering problems," IEEE Trans. Antennas Propag. **40**, 7–12 (1992).
34. R. Coifman, V. Rokhlin, and S. Wandzura, "The fast multipole method for the wave equation: a pedestrian description," IEEE Trans. Antennas Propag. **35**, 634–641 (1993).
35. D. J. Donohue, H.-C. Ku, and D. R. Thompson, "Application of iterative moment-method solutions to ocean surfaces radar scattering," IEEE Trans. Antennas Propag. **46**, 121–132 (1998).
36. J. A. Sánchez-Gil, A. A. Maradudin, J. Q. Lu, V. D. Freilikher, M. Pustilnik, and I. Yurkevich, "Scattering of electromagnetic waves from a bounded medium with random surface," Phys. Rev. B **50**, 15353–15368 (1994).
37. A. Madrazo and A. A. Maradudin, "Numerical solutions of the reduced Rayleigh equation for the scattering of electromagnetic waves from rough dielectric films on perfectly conducting substrates," Opt. Commun. **134**, 251–263 (1997).
38. Y. Saad, *Iterative Methods for Sparse Linear Systems* (PWS Publishing, 1996), Chap. 10.
39. I. Simonsen and A. A. Maradudin, "Numerical simulation of electromagnetic wave scattering from planar dielectric films deposited on rough perfectly conducting substrates," Opt. Commun. **162**, 99–111 (1999).
40. M. Saillard and D. Maystre, "Scattering from metallic and dielectric rough surfaces," J. Opt. Soc. Am. A **7**, 982–990 (1990).
41. M. Saillard and D. Maystre, "Scattering from random rough surfaces: a beam simulation method," J. Opt. (Paris)19, 173–176 (1988).
42. X. Wang, C.-F. Wang, Y.-B. Gan, and L.-W. Li, "Electromagnetic scattering from a circular target above or below rough surface," Electromagn. Waves **40**, 207–227 (2003).